Estimating source position accuracy of a large-aperture hydrophone array for bioacoustics

Magnus Wahlberg,[a] Bertel Møhl, and Peter Teglberg Madsen
Center for Sound Communication, Department of Zoophysiology, Århus University, Building 131,
C.F. Møllers Alle, DK-8000 Århus C, Denmark

A linear error propagation analysis was applied to a hydrophone array used to locate sperm whales [see Møhl *et al.*, J. Acoust. Soc. Am. **107**, 638–648 (2000)]. The accuracy of two-dimensional (2D) and three-dimensional (3D) array configurations was investigated. The precision in source location was estimated as a function of inaccuracies in measurements of sound velocity, time-of-arrival differences (TOADs), and receiver positions. The magnitude of additional errors caused by geometric simplification was also assessed. The receiver position uncertainty had the largest impact on the precision of source location. A supplementary vertical linear array consisting of three receivers gave information on the vertical bearing and distance to the sound sources. The TOAD data from an additional receiver as well as from surface reflections were used to form an overdetermined location system. This system rendered positions within two standard deviations of the estimated errors from the original 3D array. © *2001 Acoustical Society of America.*
[DOI: 10.1121/1.1329619]

LIST OF SYMBOLS AND ABBREVIATIONS

A	data matrix
δc, δs_x, etc.	error (1 s.d.) of sound velocity, source position x coordinate, etc.
b	data vector
B, $B30$	platform B; 30-m hydrophone at platform B
c	sound velocity
Cov(**b**)	covariance matrix of vector **b**
$E1–E5$	detonators 1–5
G, $G30$	platform G, 30-m hydrophone at platform G
GPS	Global Positioning System
m	source solution vector
MINNA	minimum number of receiver array
M, $M30$	platform M; 30-m hydrophone at platform M
N, $N30$	platform N; 30-m hydrophone at platform N
m_r	number of receivers
ODA	overdetermined array
PLA	perturbed linear array
R	receiver coordinate matrix
R, $R30$	platform R; 30-m hydrophone at platform R
r(1)–**r**(5)	receiver 1–5 coordinates
s	source position vector
s.d.	standard deviation
SVP	sound velocity profile
TOAD	time-of-arrival difference

I. INTRODUCTION

Acoustic locationing is a common technique in bioacoustics using a set of receivers (a receiver array). Usually a minimum number of receiver array (MINNA) is used. A MINNA implies that the array consists of the smallest number of receivers required to find the source location. To restrict the source to a hyperboloid surface,[1] one time-of-arrival difference (TOAD) is needed, and therefore the MINNA system consists of two receivers. To calculate the source position in 2D (two dimensions), one has to estimate two coordinates, or two independent parameters. Therefore, two TOADs are needed, and the MINNA system consists of three receivers. The same argument gives a MINNA system of four receivers when solving a 3D source location problem.[2] If there are more receivers present than what is needed for the MINNA solution, the system is denoted an overdetermined array (ODA).

It is essential to know the precision of the derived source coordinates in acoustic location studies. Location errors are induced by uncertainties in the variables used for calculating the source position, such as the sound and wind (current) velocity of the medium, time of arrivals, and receiver position coordinates. In MINNA systems the number of TOAD data is just sufficient to calculate the source position, and there are no extra TOAD data available to evaluate the precision. However, if the errors in the measured variables (sound velocity, TOADs, and receiver positions) are assessed, the magnitude of the error in source position can still be determined. The simplest methods for such an error assessment is linear error propagation (Taylor, 1997). Consider a function of N variables $f = f(x_1, x_2, \ldots x_N)$. Assume that the errors δx_i of the variables x_i ($i = 1, \ldots, N$) can be assessed. The linear error propagation model estimates the magnitude of the error in f (denoted δf) as

$$\delta f = \sqrt{\sum_{i=1}^{N} \left(\frac{\partial f}{\partial x_i} \delta x_i \right)^2}. \tag{1}$$

[a] Electronic mail: Magnus.Wahlberg@biology.au.dk
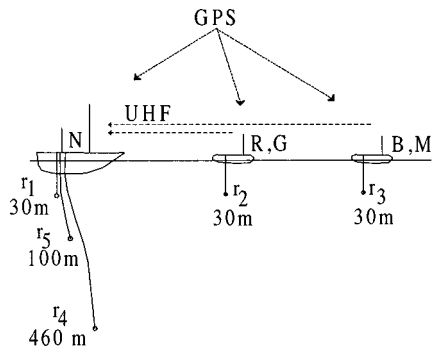
FIG. 1. The recording principle used for positioning sperm whales. Abbreviations: r=receiver, with identification and depth. GPS=Global Positioning System, UHF=Ultrahigh frequency radio link. N=main platform, G,M=auxiliary platforms in 1997, R,B=auxiliary platforms in 1998. For the recordings made in 1997, receivers 4 and 5 were not available.

If the variables x_i are correlated, Eq. (1) is modified with additional terms containing the covariances between the x_i's (Taylor, 1997).

The literature on error analysis of acoustic location systems is vast. However, for the common bioacoustic arrays with a limited amount of receivers, there are only a few examples where an error analysis has been performed. Smith *et al.* (1998) and Aubauer *et al.* (2000) performed error analyses of 2D MINNA systems, and Janik *et al.* (2000) compared acoustic- with telemetry-derived positions. Watkins and Schevill (1971) outlined an error analysis for TOAD measurement, and Cleator and Dueck (1995) made measurements on positioning error of a 3D MINNA. In this paper we extend Watkins and Schevill's (1971) approach to formulate a linear error propagation model for all the types of errors encountered when determining the position of a source. Only the wind (or current) field is not considered. The problem of wind fields has been treated extensively by other investigators (such as Spiesberger and Fristrup, 1990). The model presented here can be used for both 2D and 3D MINNA or ODA systems. It is exemplified on data on sperm whale acoustic source location presented in Møhl *et al.* (2000a).

II. METHODS

A. Field recordings

Recordings were made off the continental shelf of Northern Norway (N69°23,E15°45) in the presence of an unknown number of sperm whales during July 1997 and July 1998. In the recording area, the seafloor drops rapidly from a depth of 130 m to more than 1 km. All recordings were made in sea state 2 or below. The recording setup is described in Møhl *et al.* (2000a). In the present paper only facts relevant for estimating the precision of source positions are given. The setup is schematically outlined in Fig. 1. The array consisted of three free-floating platforms (labeled as in Møhl *et al.*, 2000a: main craft N in both 1997 and 1998, and auxiliary crafts G and M in 1997, R and B in 1998), each equipped with a hydrophone at 30 m depth. In 1998, two additional hydrophones were lowered from the N craft to depths of 100 and 460 m (receiver 4 and 5 in Fig. 1). The

hydrophone signals from the two auxiliary crafts were transmitted via UHF links to the main platform. On the main platform all hydrophone signals were recorded on a Racal Store 7D multichannel instrumentation recorder. The bandwidth (-3-dB limits) of the recorded signals was 2 kHz for the radio links and 37.5 kHz for the direct recordings on the N craft. The signals were subsequently low-pass filtered (20 kHz) and digitized using a PC sound card (sampling frequency 44.1 kHz, 16-bit resolution). The position of each craft was logged every 2 s using the Global Positioning System (GPS; Garmin GPS45 receivers). Additional radar measurements of platform distances were made from the main craft at irregular intervals. In 1998, the receiver positions were calibrated using three detonators fired 3–20 m below each craft. Two additional detonators were set off 3 m below a fourth craft. The sound velocity profile (SVP) from the surface to a depth of 150 m was measured in 1998 with a custom-built *sing-around* sound velocimeter (Urick, 1983). The SVP at greater depths was calculated from salinity and temperature measurements made in the same general area during July 1997 and July 1998 (obtained from the Institute of Marine Research, Bergen, Norway).

B. Source location algorithms

Whales were located from TOADs of the same click recorded on the different receivers. TOADs were measured with a two-channel sound-editing program. Four different source location algorithms were used.

(1) A 2D MINNA algorithm was used with the 1997 field data (receivers 1–3 in Fig. 1).
(2) A 3D MINNA algorithm was used with the 1998 field data (receivers 1–4 in Fig. 1).
(3) A vertical linear array was analyzed with data from the three receivers on the N platform in 1998 (receivers 1, 4, and 5 in Fig. 1).
(4) An ODA algorithm was used with data from all five receivers in Fig. 1 as well as from surface reflections (1998 field data).

There are several mathematical ways to solve the source location problem (Watkins and Schevill, 1971; Rindorf, 1981; Spiesberger and Fristrup, 1990; Juell and Westerberg, 1993). The algebraic solution presented here is a synthesis of the methods used by Watkins and Schevill (1971) and Spiesberger and Fristrup (1990). It has the advantage of giving the same mathematical form for 2D and 3D array systems, and for both MINNAs and ODAs.

In the following, boldface letters indicate column vectors or matrices, and $^\mathbf{T}$ denotes the transpose operator. For a source with position vector $\mathbf{s}=(s_x,s_y,s_z)^\mathbf{T}$ the distances between the source and the receivers give the equations

$$(r_x(i)-s_x)^2+(r_y(i)-s_y)^2+(r_z(i)-s_z)^2$$
$$=c^2(T_1+t(i))^2, \quad i=1,2,3,mr, \quad (2)$$

where the receiver position vector of receiver i is $\mathbf{r}(i)$ $=(r_x(i),r_y(i),r_z(i))^T$, c is the sound velocity, $t(i)$ is the TOAD between receiver i and receiver 1, and m_r is the number of receivers. The time of arrival from the source to the

receiver 1 is denoted T_1. Placing the origin of the coordinate system at $\mathbf{r}(1)$, and subtracting the $i=1$ row from the other rows in Eq. (2), we obtain (Spiesberger and Fristrup, 1990)

$$\mathbf{Am} = \mathbf{b}. \tag{3}$$

The ith row of the matrix $\mathbf{A}$ is given by $2[\mathbf{r}(i+1)^T \ c^2 t(i+1)]$, where $\mathbf{r}(i)$ is the position vector of the ith receiver, c is the sound velocity of the medium, and $t(i)$ is the TOAD between the ith and the first receiver $(i=1,...,m_r-1)$. The vector $\mathbf{m}$ is given by $[\mathbf{s}^T T_1]^T$, where $\mathbf{s}=(s_x,s_y,s_z)^T$ is the source position vector, T_1 is the straight-line travel time from the source to receiver 1. The ith row of matrix $\mathbf{b}$ is given by $b_i = -c^2 t^2(i+1) + \|\mathbf{r}(i)\|^2$, where $\|\mathbf{r}(i)\|$ denotes the length of the vector $\mathbf{r}(i)$.

The task is now to solve Eq. (3) for the vector $\mathbf{m}$, which contains the source coordinates.

For a 3D MINNA system, $m_r=4$. Below, Watkins and Schevill's (1971) solution is reformulated in matrix notation, which facilitates the error analysis notation. Equation (3) may be written as

$$2\mathbf{R}^T\mathbf{s} + 2c^2\mathbf{t}T_1 = \mathbf{b}. \tag{4}$$

Here, $\mathbf{R}$ denotes the receiver matrix

$$\mathbf{R} = \begin{pmatrix} r_x(2) & r_x(3) & r_x(4) \\ r_y(2) & r_y(3) & r_y(4) \\ r_z(2) & r_z(3) & r_z(4) \end{pmatrix},$$

and $\mathbf{t} = [t(2) \ t(3) \ t(4)]^T$. It follows that

$$\mathbf{s} = -c^2\mathbf{R}^{-T}\mathbf{t}T_1 + \tfrac{1}{2}\mathbf{R}^{-T}\mathbf{b}. \tag{5}$$

Using the relationship $c^2 T_1^2 = \mathbf{s}^T\mathbf{s}$, we solve for T_1

$$T_1 = \frac{-p \pm \sqrt{p^2 - aq}}{a}, \tag{6}$$

where $a = c^4\mathbf{t}^T\mathbf{R}^{-1}R^{-T}\mathbf{t} - c^2$, $p = -c^2\mathbf{t}^T\mathbf{R}^{-1}\mathbf{R}^{-T}\mathbf{b}/2$, and $q = \mathbf{b}^T\mathbf{R}^{-1}\mathbf{R}^{-T}\mathbf{b}/4$. Equation (5) can now be solved to give the coordinates of the source.

Each set of TOADs will result in two T_1's from Eq. (6). A negative T_1 is discarded as noncausal. Two positive solutions correspond to two source positions for the given set of TOADs. If T_1 is complex there is no physical source solution.

For a 2D MINNA system, all terms with $i=4$ and z indices in Eqs. (5)–(6) are omitted.

With a linear array, the bearing and range to the source can be found in a similar manner (Møhl et al., 1990). The three-receiver vertical linear array analyzed in this paper had the positions of the receivers $\mathbf{r}(4)$ and $\mathbf{r}(5)$ shifted from the vertical axes, and the three receivers were not on a line. This receiver geometry is called a perturbed linear array (PLA). With this array the intersection of the two rotated hyperboloids is not symmetric around the vertical axes. A numerical routine was constructed to plot the hyperboloid intersections. First, a vertical plane was defined in the direction from receiver $\mathbf{r}(1)$ and the source (as obtained from the 3D algorithm). The intersection of the this plane and the hyperbo-

loids was plotted, and the point where the two intersection lines crossed was estimated from the plot and compared with the 3D solution.

For ODA systems, the least-square solution to Eq. (3) is obtained as

$$\mathbf{m} = \mathbf{VS}^*\mathbf{U}^T\mathbf{b}, \tag{7}$$

where $\mathbf{S}^* = (\underline{\mathbf{S}}^{-1}\mathbf{0})^T$ and $\mathbf{S} = (\underline{\mathbf{S}}\mathbf{0})^T$, and $\mathbf{A} = \mathbf{USV}^T$ is the singular value decomposition of the matrix $\mathbf{A}$ (Spiesberger and Fristrup, 1990).

C. The linear error propagation model

First, consider a MINNA system. Watkins and Schevill (1971) used a linear error propagation model on their 3D location algorithm with respect to uncertainties in TOAD measurements. Here, we expand their analysis to incorporate the impact on location errors caused by other measured variables, such as sound velocity and receiver positions. The analysis presented here also allows the effect of correlations between measured variables to be investigated. The analysis results in a covariance matrix for the source position vector, Cov($\mathbf{s}$), containing the estimated variances for each source coordinate in its diagonal, and the covariances between different source coordinates in the off-diagonal places. The total error is defined as the square root of the trace of the covariance matrix.

The covariance matrix for the source position vector is estimated as

$$\text{Cov}(\mathbf{s}) = \left(\frac{d\mathbf{s}}{d(c,\mathbf{t},\mathbf{R})}\right)^T \text{Cov}(c,\mathbf{t},\mathbf{R})\left(\frac{d\mathbf{s}}{d(c,\mathbf{t},\mathbf{R})}\right), \tag{8}$$

where $(c,\mathbf{t},\mathbf{R})$ denotes a vector containing the c, $\mathbf{t}$, and $\mathbf{R}$ elements. Vector derivatives are defined as in Wunsch (1996). For the uncorrelated variables c, $\mathbf{t}$, and $\mathbf{R}$, Eq. (8) can be split up into

$$\text{Cov}(\mathbf{s}) = \left(\frac{d\mathbf{s}}{dc}\right)^T \text{Cov}(c)\left(\frac{d\mathbf{s}}{dc}\right) + \left(\frac{d\mathbf{s}}{d(\mathbf{t})}\right)^T \text{Cov}(\mathbf{t})\left(\frac{d\mathbf{s}}{d(\mathbf{t})}\right)$$
$$+ \left(\frac{d\mathbf{s}}{d(\mathbf{R})}\right)^T \text{Cov}(\mathbf{R})\left(\frac{d\mathbf{s}}{d(\mathbf{R})}\right). \tag{9}$$

The terms on the right-hand side in Eq. (9) correspond to the contribution to the source position error from the inaccuracies in sound velocity, TOADs, and receiver position measurements, respectively.

The covariance matrix for c is simply δc^2, where δc is the standard deviation in the sound velocity estimate. The error analysis is performed analogous to Eq. (11) below.

Each TOAD is measured between the time of arrival at receiver 1 and receiver i. Assume that the time of arrivals are uncorrelated and associated with an equal measurement inaccuracy of δt (1 s.d.). Then the TOADs all include T_1 and are correlated with the amount δt^2. We obtain the TOAD covariance matrix as

$$\text{Cov}(\mathbf{t}) = \begin{bmatrix} 2 & 1 & 1 \\ 1 & 2 & 1 \\ 1 & 1 & 2 \end{bmatrix} \delta t^2. \tag{10}$$

The derivatives of **s** in Eq. (9) are

$$\frac{d\mathbf{s}}{d\mathbf{t}} = -c^2\left(T_1 + \mathrm{diag}(\mathbf{t}) + \frac{\partial T}{\partial \mathbf{t}}\mathbf{t}^T\right)\mathbf{R}^{-1},$$

$$\frac{\partial T}{d\mathbf{t}} = \frac{-d_t p \pm \dfrac{2p\dfrac{\partial p}{\partial \mathbf{t}} - a\dfrac{\partial q}{\partial \mathbf{t}} - q\dfrac{\partial a}{\partial \mathbf{t}}}{2\sqrt{p^2 - aq}} - T_1\dfrac{\partial a}{\partial \mathbf{t}}}{a},$$

$$\frac{\partial p}{\partial \mathbf{t}} = c^4\,\mathrm{diag}(\mathbf{t})\mathbf{R}^{-1}\mathbf{R}^{-T}\mathbf{t} - \frac{c^2}{2}\mathbf{R}^{-1}\mathbf{R}^{-T}\mathbf{b}, \qquad (11)$$

$$\frac{\partial q}{\partial \mathbf{t}} = -c^2\,\mathrm{diag}(\mathbf{t})\mathbf{R}^{-1}\mathbf{R}^{-T}\mathbf{b},$$

$$\frac{\partial a}{\partial \mathbf{t}} = 2c^4\mathbf{R}^{-1}\mathbf{R}^{-T}\mathbf{t},$$

where $\mathrm{diag}(\mathbf{t})$ is a square 3×3 diagonal matrix with the elements of **t** in the diagonal.

The evaluation of the receiver term in Eq. (9) is made through the decomposition (receiver x, y, and z coordinates are assumed to be uncorrelated)

$$\left(\frac{d\mathbf{s}}{d(\mathbf{R})}\right)^T \mathrm{Cov}(\mathbf{R})\left(\frac{d\mathbf{s}}{d(\mathbf{R})}\right)$$

$$= \sum_{j=x,y,z}\left(\frac{d\mathbf{s}}{dr_j}\right)^T \mathrm{Cov}(\mathbf{r}_j)\left(\frac{d\mathbf{s}}{dr_j}\right). \qquad (12)$$

Each receiver coordinate is determined as the distance between the receiver i and receiver 1 in the coordinate direction. Each receiver coordinate is therefore correlated with the same coordinate of another receiver with the amount $\delta r_j(1)^2$. This gives the receiver covariance matrices

$$\mathrm{Cov}(r_j) = \begin{bmatrix} \delta r_j(1)^2 + \delta r_j(2)^2 & \delta r_j(1)^2 & \delta r_j(1)^2 \\ \delta r_j(1)^2 & \delta r_j(1)^2 + \delta r_j(3)^2 & \delta r_j(1)^2 \\ \delta r_j(1)^2 & \delta r_j(1)^2 & \delta r_j(1)^2 + \delta r_j(4)^2 \end{bmatrix}, \quad j=x,y,z. \qquad (13)$$

The derivatives are found in a similar fashion to Eq. (11).

For the ODA solution [Eq. (7)] the error in the least-square approximation can be estimated either through linear error propagation or residual analysis. Linear error propagation is chosen for direct comparison with the MINNA analysis. Spiesberger and Fristrup (1990) used this technique for the case of TOAD measurement errors. Here, the same analysis is extended to measurement errors in sound velocity and receiver positions. The resulting covariance matrix for **m** contains the variances $\delta\mathbf{m}^2 = (\delta s_x^2, \delta s_y^2, \delta s_z^2, \delta T_1^2)^T$ in the diagonal. The total error is defined as the square root of the sum of δs_x^2, δs_y^2, and δs_z^2.

Analogous to the MINNA analysis, the covariance matrix of **m** for ODA is

$$\mathrm{Cov}(\mathbf{m}) = \mathbf{V}\mathbf{S}^*\mathbf{U}^T\mathrm{Cov}(\mathbf{b})\mathbf{U}(\mathbf{S}^*)^T\mathbf{V}^T, \qquad (14)$$

where the covariance matrix of **b** is split up into its uncorrelated terms

$$\mathrm{Cov}(\mathbf{b}) = \left(\frac{d\mathbf{b}}{dc}\right)^T\mathrm{Cov}(c)\left(\frac{d\mathbf{b}}{dc}\right) + \left(\frac{d\mathbf{b}}{d(\mathbf{t})}\right)^T\mathrm{Cov}(\mathbf{t})\left(\frac{d\mathbf{b}}{d(\mathbf{t})}\right)$$

$$+ \left(\frac{d\mathbf{b}}{d(\mathbf{R})}\right)^T\mathrm{Cov}(\mathbf{R})\left(\frac{d\mathbf{b}}{d(\mathbf{R})}\right). \qquad (15)$$

The covariance matrix of the sound velocity is given simply by δc^2, the variance of the sound velocity estimate. The components of $\partial\mathbf{b}/\partial c$ are

TABLE I. Estimated error (1 s.d.) of variables used in source positioning of the Møhl et al. (2000) data.

Variable/ source of error	Assumed error 1997	Assumed error 1998	Comments
Sound velocity	±10 m/s	±10 m/s	From sound velocity profile data
Time of arrival	±0.001 s	±0.001 s	Measurement accuracy of click timing
$r_1 x,y,z$ coordinate	±0 m	±0 m	Defines origin of coordinate system
$r_2 x$ coordinate	±70 m	±20–60 m	Estimated from GPS data and detonators
$r_2 y$ coordinate	±0 m	±0 m	Defines direction of x axis
$r_3 x,y$ coordinate	±300 m	±20–60 m	From radar, GPS, and detonators
$r_4 x,y$ coordinates	⋯	±10–60 m	From GPS and detonators
$r_5 x,y$ coordinates	⋯	±10–60 m	From GPS and detonators
$r_2, r_3 z$ coordinates	⋯	±2 m	From detonators
$r_4 z$ coordinate	⋯	±20–60 m	From detonators
$r_5 z$ coordinate	⋯	±20–50 m	From detonators
2D simplification	⋯	⋯	Magnitude of error depends on source–array geometry
Ray bending	⋯	⋯	Magnitude of error depends on source–array geometry

$$\frac{\partial b_i}{\partial c} = -2ct(i)^2. \tag{16}$$

The covariance matrix of $\mathbf{t}$ is given by

$$\mathrm{Cov}(\mathbf{t}) = \begin{bmatrix} 2 & 1 & \cdots & & 1 \\ 1 & 2 & & & \vdots \\ \vdots & & \ddots & & \vdots \\ \vdots & & & 2 & 1 \\ 1 & \cdots & \cdots & 1 & 2 \end{bmatrix} \delta t^2, \tag{17}$$

$$\mathrm{Cov}(r_j) = \begin{bmatrix} \delta r_j(1)^2 + \delta r_j(2)^2 & \delta r_j(1)^2 & \cdots & & \cdots & \delta r_j(1)^2 \\ \delta r_j(1)^2 & \delta r_j(1)^2 + \delta r_j(3)^2 & & & & \vdots \\ \vdots & & \ddots & & & \vdots \\ \vdots & & & \delta r_j(1)^2 + \delta r_j(m_r-1)^2 & \delta r_j(1)^2 & \vdots \\ \delta r_j(1)^2 & \cdots & \cdots & \delta r_j(1)^2 & \delta r_j(1)^2 + \delta r_j(m_r)^2 \end{bmatrix}, \quad j = x, y, z. \tag{19}$$

The derivatives of $\mathbf{b}$ are found as

$$\frac{\partial b_i}{\partial r_j(k)} = 2c^2 r_j(i) \delta_{ik}, \tag{20}$$

with the Dirac delta function δ_{ij} defined as above.

D. Sources of errors for acoustic location

Table I lists the sources of errors in variables used to calculate source positions in the Møhl *et al.* (2000a) data.

1. Linear error propagation variables

a. Sound velocity measurement. The measured SVP (Fig. 2) decreased from 1495 m/s at the surface to 1478 m/s at a depth of 500 m. At a depth of 800 m, the sound velocity reached a minimum of 1460 m/s. In the location algorithms a sound velocity value of 1480 m/s was used, as this is the average sound velocity for a signal traveling from a source at a depth of a few hundred meters to the receivers. In the linear error propagation model the standard deviation of the sound velocity estimate was set to ± 10 m/s, which reflects the variation observed in Fig. 2.

b. TOAD measurement. The standard deviation of TOAD measurements was set to 1 ms. Sperm whale clicks have well-defined onsets, and therefore TOADs can be measured with higher precision than 1 ms. However, the precision in timing degrades due to the use of radio links of limited bandwidth and dynamic range. There are several techniques to improve the TOAD measurements (e.g., cross correlation; Cahlander, 1967; Menne and Hackbarth, 1986). As the TOAD measurement errors turned out to have an insignificant impact on source location precision in the Møhl *et al.* (2000a) data, no effort was made to make such improvements. Water currents (maximum 1–2 knots in the

where δt is the standard deviation of the TOAD measurements [cf. Eq. (10)]. The time derivatives of $\mathbf{b}$ are

$$\frac{\partial b_i}{\partial t_j} = -2c^2 t(i) \delta_{ij}, \tag{18}$$

where δ_{ij} is the Dirac delta function ($\delta_{ij} = 0$ if $i <> j$, $\delta_{ij} = 1$ if $i = j$).

The covariance matrix of the receiver positions, for the same arguments given for Eq. (13), is

present study) induce errors in TOAD measurements in the sub-ms range in the array data analyzed and were therefore not taken into account.

c. Receiver position errors. The x and y coordinates of receivers 1–3 were determined with GPS (1 s.d. positioning error ± 50 m; Kaplan, 1996), sampled with 2-s intervals. In 1997 the GPS position of receiver 3 was not recorded due to a technical failure, and the position of this craft was obtained by means of observations on a radar screen. This increased the estimated error for the coordinates of receiver 3 as compared with receiver 2 (Table I). The receiver positions from 1998 were treated in three steps to minimize the impact of fluctuations in the logged positions (Fig. 3): (1) The distances between the three platforms were calculated as a function of time; (2) Linear regression lines were fitted to each of the receiver distance curves; and (3) The regression lines
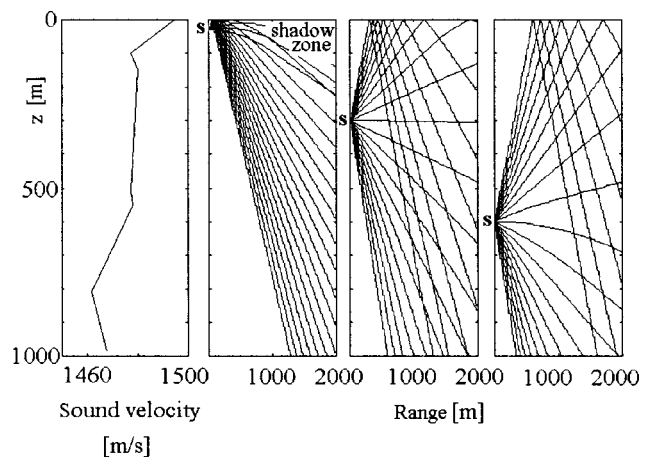
FIG. 2. The average sound velocity profile calculated from salinity and temperature measurements in the study area during July 1997 and July 1998, by the Institute of Marine Research, Bergen, Norway. Ray tracing of a sound source at depths of 30, 300, and 600 m. Ray separation: 8 degrees.
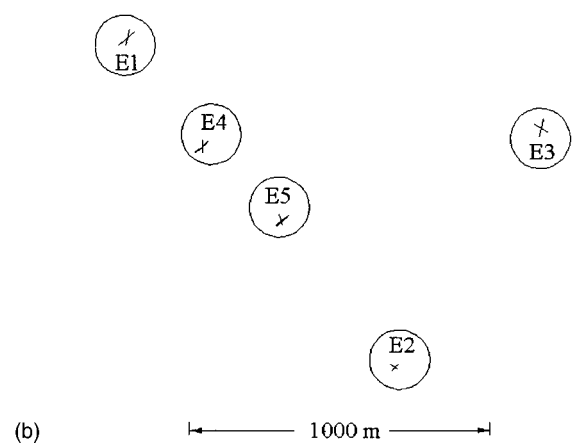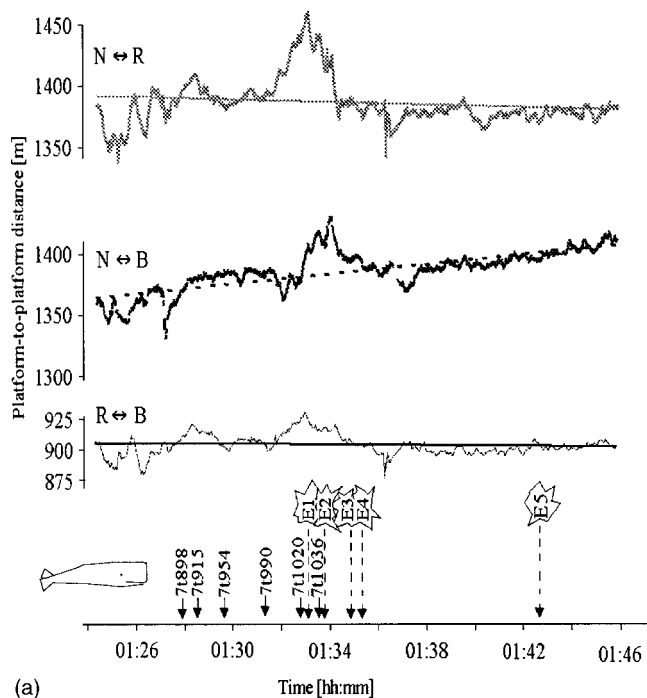
FIG. 3. (a) Distance between platforms as a function of time during the 1998 recordings. The linear regression lines for each platform distance are indicated. Six whale sequences and the detonators $E1-E5$ are indicated. (b) Calibration of recording geometry during 1998. Numbers refer to detonators $E1-E5$. Circles signify the GPS positions of the platforms, with the centers obtained through the linear regression given in Fig. 6(a). The diameter represents the 2-s.d. uncertainty in platform positions. The crosses at $1-3$ are constructed from distances derived from the time of arrivals of the detonator signals to the platforms. The crosses at 4 and 5 are derived from acoustic localization of the detonators $E4-E5$. From: Møhl *et al.* (2000a), courtesy of the *Journal of the Acoustical Society of America*.

were shifted up to 30 m using the detonator data. The array geometry at the time of a whale sequence was estimated from the adjusted regression lines.

2. Errors due to geometric simplification

a. Using a 2D algorithm in a 3D source–array geometry. A geometric problem with 2D arrays occurs when the sound source is outside the plane defined by the receivers (Konagaya, 1982; Stæhr, 1982). As sketched in Fig. 4(a), the projection of the 3D position of the sound source onto the receiver plane may differ considerably from the coordinates obtained with the 2D solution. The implication of this error is that a position estimate made with a 2D algorithm is either
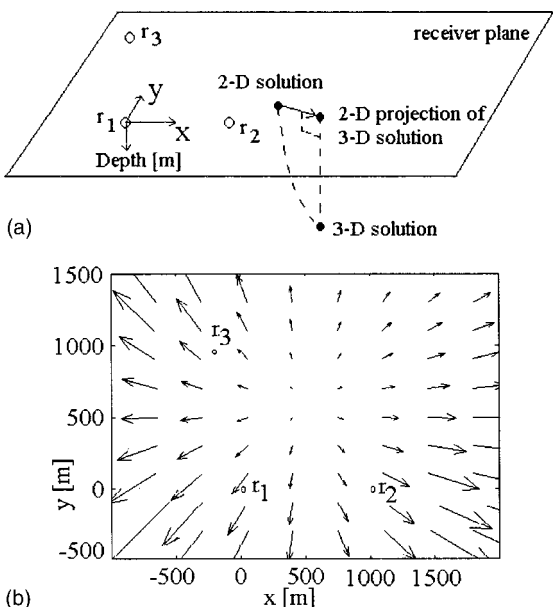
FIG. 4. (a) Illustration of the positioning error produced by locating a sound source with a 2D array, when the actual position of the source (denoted 3D solution) is not situated on the receiver plane. (b) Magnitude and direction of this error from the 1997 data. Depth of sound source: 500 m. The arrow shows the magnitude and direction of the difference between the 2D solution and the 2D projection of the 3D solution.

under- or overestimating the distances between the source and the receivers. The magnitude of this bias increases as the distance between the sound source and the receiver plane increases. In Fig. 4(b) the situation for the 2D array used in the 1997 field work is depicted for a sound source at 500 m depth.

b. Ray bending. All the location algorithms used here assume that the signal is traveling along a straight line from the source to the receiver. If the sound velocity changes with depth or otherwise, the actual sound path bends (Fig. 2; Urick, 1983). The measured TOADs then differ from those from straight path propagation. Spiesberger and Fristrup (1990) deduced an approximate formula for the deviation in time of arrival (δT) between the curved and straight path in the case of sound velocity changing linearly with depth

$$\delta T = -\left(\frac{\partial c(z)}{\partial z}\right)^2 \frac{L^3}{24c_1^3}, \qquad (21)$$

where $\partial c(z)/\partial z$ is the slope of the sound velocity profile, L is the distance between the source and the receiver, and c_1 is the sound velocity at the source depth.

E. Calibration of array configuration

The receiver array used in 1998 was calibrated using two detonators set off at 3 m depth from a separate, GPS-positioned, dinghy. The TOAD data from these detonators were used to compare acoustically derived locations with GPS positions.
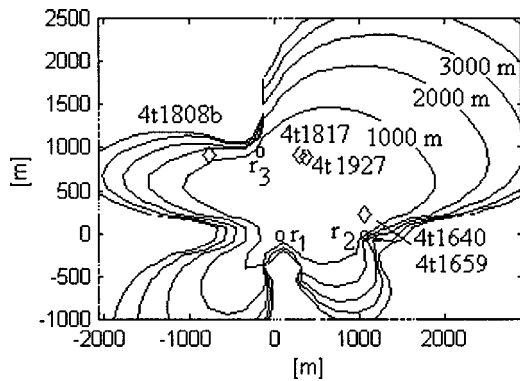
FIG. 5. Magnitude of the error in source position due to uncertainties in measurements of TOADs, sound velocity, and receiver positions applied to the 2D array data from 1997. $r(1)-r(3)$: receivers. Contour lines (spaced 1000 m) indicate the one standard deviation positioning error in m. Positions (diamonds) of five sperm whales are indicated ($4t1640$ and $4t1659$ are at the same position).

FIG. 6. Array geometry of the 1998 recordings reported in Møhl *et al.* (2000). Receivers $r(1)-r(5)$ are indicated. The positions of six whale sequences are shown as diamonds. Sequences $7t898$, $7t915$, and $7t1036$ are in a location of the array, where two source positions are found from the set of TOADs (denoted $7t1036.1$, etc.; $7t898.2$ and $7t915.2$ are outside the range of the figure). Detonations $E1-E5$ are indicated.

III. RESULTS

A. Indentifying click sequences

Click sequences were identified across receivers as consecutive clicks having the same (within 1 ms) interclick intervals on all receivers. Five click sequences from 1997 and six sequences from 1998 were analyzed. The shortest sequence consisted of five consecutive clicks, and the longest of 64. Click sequences are labeled as in Møhl *et al.* (2000a).

B. Error map of the 2-D MINNA

In Fig. 5, the result of the linear error propagation model for the 2D hydrophone array used in 1997 is shown. The contour lines (spaced 1000 m apart) indicate the magnitude of the location error (1 s.d.), using the variable errors listed in Table I. The source position of five click sequences are indicated (the sequences $4t1640$ and $4t1659$ are so close to each other that only one position is indicated). In Table II, the results from the linear error propagation model are shown for one of the whales ($4t1659$). This sequence is chosen to illustrate the error propagation analysis for a source outside the array, close to the line connecting two receivers. Errors are given in percent as the ratio of the error and the estimated source distance to $\mathbf{r}(1)$. Assuming that the whale is not situated deeper than 500 m, the maximum impact on geometric simplification is also given in Table II. Three of the sequences in Fig. 5 ($4t1640$, $4t1659$, and $4t1808b$) are situated in areas where the location error is very large. Two pairs of sequences ($4t1640-4t1659$, and $4t1817-4t1927$) almost

overlap in their positions, indicating that they are from the same whale. Thus, the five sequences probably are produced by three individual whales.

C. Error of the 3D array used in 1998

Figure 6 shows the array system used in 1998. The positions of six whale sequences are indicated, as well as the positions of the five detonators fired from the platforms and an additional dinghy. The time elapsed from the first whale sequence ($7t898$) to the last transient event ($E5$) is 14 min. The sequences were probably generated by three individual whales (1: sequences $7t1036$ and $7t898$; 2: $7t954$, $7t990$, and $7t1020$; and 3: $7t915$). In Table II, the coordinates of two of the six click sequences are listed, together with the results of the error analysis.

The $E1-E3$ detonators were also used to position the deep hydrophones $\mathbf{r}(4)$ and $\mathbf{r}(5)$. In Table III, the results are presented, as well as the errors from a linear error propagation analysis.

The TOAD measurements from the two detonators $E4-E5$ were used to compare GPS and acoustic positions. The acoustically derived positions did not deviate more than 40 m from the GPS positions of the detonators.

D. Positions from the PLA compared with 3D positions

For the PLA, the intersection of each hyperboloid and the vertical plane between receiver 1 and the 3D-derived

TABLE II. The impact on source position accuracy from errors in sound velocity, TOAD measurements, and receiver positions. The sequence $7t898$ has 2 solutions. Errors are given in percent of the ratio between the standard deviation error estimates and the derived distance between the whale and the origin of the array. Geometric error is calculated for a source depth of 500 m.

Whale	Position (x,y,z) [km]	Sound velocity error [%]	TOAD error [%]	Receiver position error [%]	3D to 2D geometric error [%]	Ray curvature error [%]
$4t1659$	1.0, 0.2, −	0.6	0.4	300	30	⋯
$7t898.1$	−0.5, −0.4, 0.2	20	2	500	⋯	3
$7t898.2$	−27, −13, 0.8	700	80	4000	⋯	⋯
$7t990$	0.3, −1.4, 0.3	5	0.2	50	⋯	0.5

TABLE III. Positions of the two deep hydrophones deployed from the N craft derived from detonators $E1-E3$.

Receiver	x [m]	y [m]	z [m]
$r(4)$	23 ± 20	-59 ± 60	462 ± 10
$r(5)$	-2 ± 20	37 ± 50	98 ± 30

whale position are shown in Fig. 7. The curves are not symmetric around the $r1-r(i)$ axis, as this axis is not running on the whale–receiver 1 plane. The 3D solution is on the H14 curve, as receiver 4 is part of the 3D MINNA system. The
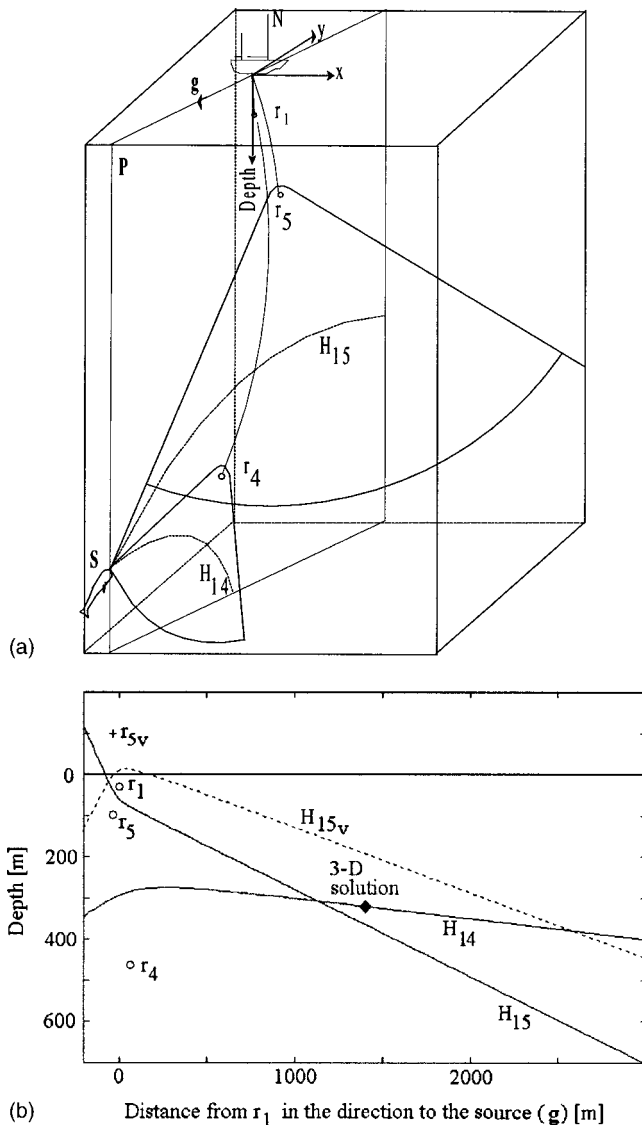
FIG. 7. (a) Geometry of the perturbed linear array analysis. x,y=coordinate system of the 3D algorithm. Abbreviations: **N**=platform. **r**(1), **r**(4), **r**(5)=receivers 1, 4, and 5. **s**=position of whale, calculated with the 3D algorithm. **g**=direction between receiver 1 and the whale in the horizontal plane. **P**=The vertical plane through **r**(1) and **s**. **H14** (**H15**): Intersection of **P** and the hyperboloid created from TOAD between receivers 1 and 4(5). (**b**) View of the receiver 1–source plane (**P** in 7a) for click sequence 7t1036. **r(4)** and **r(5)** are projections of receivers 4 and 5 onto the plane **P**. A surface reflection is treated as recorded by an additional virtual receiver, denoted **r5v**. The curves corresponding to TOADs between receivers 1–5 and 1–4 are drawn with solid lines, and the curve corresponding to TOADs between receiver 1 and the virtual receiver is drawn with a dotted line.

H15 curve is not running through the 3D solution, probably due to uncertainties in the position of receiver 5. In Table IV, the estimated ranges and bearings are compared with the 3D MINNA results for two whale sequences. The ranges and bearings calculated with the perturbed linear array are within the error margins of the 3D solution.

Several signals contained echoes, likely generated by surface reflections. Surface reflections can be viewed as recordings made by virtual hydrophones, situated above the surface at a height corresponding to the depth of the ''real'' receiver (Urick, 1983; Møhl *et al.*, 1990; Aubauer *et al.*, 2000). Surface reflection data were incorporated into the linear array analysis. The curve generated by the TOAD from a surface reflection is shown in Fig. 7(b) as a dotted curve. The dotted curve is converging reasonably well towards the 3D solution, so the corresponding echo is regarded as a surface reflection.

The surface reflected signal is expected to be 180 deg phase shifted compared with the direct signal (Urick, 1983). This should be easily observed in the cross correlation between the direct and the surface reflected signals and could thus be a further help in the interpretation of echoes. However, in the Møhl *et al.* (2000a) there was no clear negative maximum in the cross-correlation function between click and echo, so this method could not be readily implemented.

E. The ODA compared with the 3D MINNA and the PLA solutions

In Table IV, the range and bearing to the source are shown with an ODA system using receivers 1–5 and surface reflection data. Signals were considered as originating from surface reflections if the analysis with the PLA indicated that this was plausible. The ODA solution can be compared with results from the two other location algorithms: the 3D MINNA system and the PLA (Table IV). In most cases the error estimates derived with the ODA and 3D MINNA were of similar magnitude. If the source was situated outside the array close to one of its corners, the ODA errors were smaller by up to an order of magnitude (e.g., the sequence 7t898 in Table IV).

F. Errors due to a varying sound-velocity profile

The error from ray bending in five sequences from 1998 data was estimated. The source was assumed to be at the position given by the 3D solution, and Eq. (21) was used to compensate for the measured TOADs for ray-bending effects. Then, a new 3D position was calculated with the adjusted TOADs. The difference from the uncorrected positions was always less than 10% of the total error as derived from linear error propagation (Table II).

IV. DISCUSSION

The accuracy of source location depends on the precision of the measurements in sound velocity, TOADs, and receiver positions, as well as on source–array geometry. It is evident from Fig. 5 that the location precision is a complicated function of the bearing and range from the array to the source.

TABLE IV. Comparison of 3D MINNA, ODA, and PLA positioning for two click sequences selected from the 1998 data in Møhl *et al.* (2000). The sequence 7*t*898 has two solutions with the MINNA system. Range is the estimated distance from the source to receiver 1 in the origin of the array. Bearing is the angle between the horizontal plane and the line connecting the whale and receiver 1. Virtual hydrophones are constructed from signals interpreted as being reflected from the surface (see the text). The sequences are selected to illustrate the performance of the error analysis. All errors are standard deviations (± 1 s.d.).

| | 3-D MINNA | | | 3-D ODA | | | | PLA | | |
| | (Receivers 1–4) | | | (Receivers 1–5+virtual receivers) | | | | (Receivers 1, 4, and 5) | | |
Whale	Range to $r(1)$ [km]	Bearing [degrees]	Source depth [km]	No of virtual receivers	Range to $r(1)$ [km]	Bearing [degrees]	Source depth [km]	Range to $r(1)$ [km]	Bearing [deg]	Source depth [km]
7*t*898.1	0.7±3	18±80	0.2±0.5	0	0.7±0.7	16±6	0.2±0.7	0.7	18	0.2
7*t*898.2	30±90	1±60	0.8±30	···	···	···	···	···	···	···
7*t*990	1.4±0.6	11±21	0.3±0.6	2	2.3±0.5	10±4	0.4±0.1	1.1	15	0.3

A considerable problem with locating directional sources with a MINNA system is that there are no means to assure that the signal is correctly interpreted in terms of direct and reflected paths. In the present study the PLA data were used to confirm the range and vertical bearing to the source from the *N* platform. Still, there is a possibility that an erroneous interpretation of the signal TOADs can render similar yet erroneous results with the two location systems, as two of the linear array receivers were also a part of the 3D MINNA system. To some extent, surface reflections can be used to confirm the interpretation of the TOADs (Møhl *et al.*, 1990; Aubauer *et al.*, 2000). The problem can best be minimized through the use of an overdetermined system, where additional independent data are collected.

Overdetermined systems are also favorable in terms of reducing the positioning error. This effect is most clearly seen in the areas of the array where the ODA systems are very sensitive to errors (Table IV).

The linear error propagation analysis applied in this study gives a measure of the expected error in source location. The fact that the analysis is linear makes it unfeasible in areas of the array where the location error increases rapidly (i.e., nonlinearly). This is clearly seen in Table II. The estimated source location errors of the sequences 4*t*1659 and 7*t*898 are much larger than the location inaccuracies we would expect from repeated measurements of sound sources situated at these positions. Spiesberger (1999) deduced boundaries where the linear approximation of location errors breaks down for overdetermined acoustic location systems. A similar approach to MINNA systems would be useful to define the source–array geometries for which the linear error propagation analysis presented here is valid. The nonlinear effect is largest where the hyperboloid surfaces have large curvature or are almost parallel.

The PLA created with the hydrophones deployed from the *N* platform in 1998 gave additional vertical bearing and range data which proved useful to confirm source positions derived with the 3D algorithm [Fig. 7(b), Table IV]. In two end-fire situations (sequences 7*t*898 and 7*t*1036 in Fig. 5) the difference in the ranging estimation of the PLA and the MINNA solutions was within 20% of the range. The difference is readily explained by the uncertainties in the *N*100 and *N*460 receiver positions.

When cross-correlating a click with an assumed surface reflection, it was not possible to discern whether the cross-correlation function had a positive or a negative maximum.

A likely reason for this is the observed acute directionality of sperm whale clicks (Møhl *et al.*, 2000a). The direct path and surface reflected signals originate from different directions of the sperm whale transmission beam, and therefore the frequency and phase content of the two signals may differ significantly. Additionally, inhomogeneities in the water mass between the source and the various receivers may distort the signal differently.

There are two major causes for source position uncertainty in the hydrophone array system described by Møhl *et al.* (2000a): receiver position uncertainty, and the usage of a 2D array in a 3D geometry. The second problem was eliminated during the field work in 1998 through the use of a 3D array. In addition, the errors in receiver positions were reduced through acoustic calibration by the firing of detonators. The differences between acoustically derived and GPS-logged receiver positions were well within the ± 50-m error margin of the GPS system at the time [Fig. 3(b)]. This indicates that the regression performed on the GPS coordinates [Fig. 3(a)] eliminated some of the error associated with the GPS location of the platforms. The spurious jumps in the GPS locations observed in Fig. 3(a) are due to short periods where one or more of the GPS receivers lost contact with the satellites. During such circumstances the GPS receiver is estimating its position from dead reckoning. More accurate receiver positions can be obtained using differential GPS receivers (Kaplan, 1996). With such a system, the platform location error can be reduced by about one order of magnitude, leading to a similar reduction in errors in source location.

The impact of ray bending on location errors at the ranges and depths relevant for the Møhl *et al.* (2000a) data is at least an order of magnitude smaller than location errors caused by receiver position uncertainties (Table II). Figure 2 shows that the the ray tracings create no major ray bending at the distances and depths relevant for the data presented here. The largest problem with ray bending is the fact that the SVP of the present study created a shadow zone (Urick, 1983; Fig. 2) for shallow sources and receivers. This shadow zone starts a few kilometers away from the source and may cause considerable underestimation of sound levels recorded from shallow or distant whales.

The linear error propagation model is a useful tool for estimating location errors. Such an analysis can be used to obtain error estimates for derived parameters based on ranging information such as source levels (Møhl *et al.*, 2000a).

The error analysis is also an effective tool for pinpointing the factors causing the largest impact on the source position precision. This has been an important argument in developing the acoustic location systems investigated here into an over-determined acoustic location system (Møhl *et al.*, 2000b).

ACKNOWLEDGMENTS

[1]In 2D applications, the hyperboloid surface is reduced to a hyperbola curve.
[2]In some source–receiver geometries, the MINNA may render two source solutions. In these cases an extra receiver is needed to remove the ambiguity in the location of the source.

Aubauer, R., Lammers, M. O., and Au, W. W. L. (**2000**). ''One-hydrophone method of estimating distance and depth of phonating dolphins in shallow water,'' J. Acoust. Soc. Am. **107**, Pt1, 2744–2749.

Cahlander, D. (**1967**). ''Discussion,'' in *Animal Sonar Systems. Biology and Bionics*, edited by R. E. Busnel (NATO Advanced Study Institute), Vol. 2, pp. 1052–1081.

Cleator, H., and Dueck, L. (**1995**). ''Three-dimensional accuracy of a four-hydrophone array,'' 11th Biennial Conference on the Biology of Marine Mammals, 14–18 December 1995, Orlando.

Janik, V. M., van Parijs, S. M., and Thompson, P. M. (**2000**). ''A two-dimensional acoustic localization system for marine mammals,'' Marine Mammal Sci. **16(2)**, 437–447.

Juell, J.-E., and Westerberg, H. (**1993**). ''An ultrasonic telemetric system for automatic positioning of individual fish used to track Atlantic salmon (*Salmo salar L.*) in a sea cage,'' Aquacultural Eng. **12**, 1–18.

Kaplan, E. D. (editor) (**1996**). *Understanding GPS: Principles and applications*. Artech House, Inc., MA.

Konagaya, T. (**1982**). ''A new telemetric method of determining the positions of swimming fish,'' Bulletin Jpn. Soc. Scientific Fisheries **48**(11), 1545–1550.

Menne, D., and Hackbarth, H. (**1986**). ''Accuracy of distance measurement in the bat *Eptesicus fuscus*: Theoretical aspects and computer simulations,'' J. Acoust. Soc. Am. **79**, 386–397.

Møhl, B., Surlykke, A., and Miller, L. A. (**1990**). ''High intensity narhval clicks,'' in *Sensory Abilities of Cetaceans*, edited by J. A. Thomas and R. A. Kastelein (Plenum, New York), pp. 295–303.

Møhl, B., Wahlberg, M., Madsen, P. T., Miller, L. A., and Surlykke, A. (**2000a**). ''Sperm whale clicks: Directionality and source levels revisited,'' J. Acoust. Soc. Am. **107**, 638–648.

Møhl, B., Wahlberg, M., and Heerfordt, A. (**2000b**). ''A large-aperture array of nonlinked receivers for acoustic positioning of biological sound sources,'' J. Acoust. Soc. Am. (in press).

Rindorf, H. J. (**1981**). ''Acoustic emission source location in theory and in practice,'' Brüel & Kjær Technical Review No. 2.

Smith, G. W., Urquhart, G. G., MacLennan, D. N., and Sarno, B. (**1998**). ''A comparison of theoretical estimates of the errors associated with ultrasonic tracking using a fixed hydrophone array and field measurements,'' Hydrobiologia **371/372**, 9–17.

Spiesberger, J. L. (**1999**). ''Locating animals from their sounds and tomography of the atmosphere: Experimental demonstration,'' J. Acoust. Soc. Am. **106**, 837–846.

Spiesberger, J. L., and Fristrup, K. M. (**1990**). ''Passive location of calling animals and sensing of their acoustic environment using acoustic tomography,'' Am. Nat. **135**, 107–153.

Stæhr, K.-J. (**1982**). ''Passiv akustisk lokalisering af dyr. Teori og praksis,'' M.Sc. thesis, Aarhus University, Denmark (in Danish).

Taylor, J. R. (**1997**). *An introduction to Error Analysis*, 2nd ed. (University Science, Sausalito, CA), Chap. 3.

Urick, R. J. (**1983**). *Principles of Underwater Sound*, 3rd ed. (Peninsula, Los Altos, CA).

Watkins, W. A., and Schevill, W. E. (**1971**). ''Four-hydrophone array for acoustic three-dimensional location,'' Woods Hole Oceanographic Institution, Technical Report, Reference No. 71-60, unpublished manuscript.

Wunsch, C. (**1996**). *The Ocean Circulation Inverse Problem* (Cambridge University Press, New York).